RSC Advances

PAPER

View Article Online
View Journal | View Issue

Cite this: *RSC Adv.*, 2024, **14**, 22656

Precursor engineering for soft selective synthesis of phase pure metal-rich digenite (Cu_9S_5) and djurleite ($Cu_{31}S_{16}$) nanocrystals and investigation of their photo-switching characteristics†

Suraj Peerappa Yadav,‡[a] Gourab Karmakar, ‡[b] Alpa Y. Shah,[b] Bal Govind Vats, [c] Ankita Pathak,[d] Adish Tyagi, *[b] Rohit Singh Chauhan *[a] and Vishal Singh[e]

Copper sulfide nanostructures have evolved as one of the most technologically important materials for energy conversion and storage owing to their economic and non-toxic nature and superior performances. This paper presents a direct, scalable synthetic route aided by a single source molecular precursor (SSP) approach to access copper sulfide nanomaterials. Two SSPs, $CuX(dmpymSH)(PPh_3)_2$ (where X = Cl or I), were synthesized in quantitative yields and thermolyzed under appropriate conditions to afford the nanostructures. The analysis of the nanostructures through pXRD, EDS and XPS suggested that phase pure digenite (Cu_9S_5) and djurleite ($Cu_{31}S_{16}$) nanostructures were isolated from –Cl and –I substituted SSPs, respectively. The morphologies of the as-synthesized nanomaterials were investigated using electron microscopy techniques (SEM and TEM). DRS studies on pristine materials revealed blue shifted optical band gaps, which were found to be optimum for photoelectrochemical application. A prototype photoelectrochemical cell fabricated using the pristine nanostructures exhibited a stable photo-switching property, which presents these materials as suitable economic and environmentally friendly photon absorber materials.

Received 20th June 2024
Accepted 4th July 2024

DOI: 10.1039/d4ra04524f

rsc.li/rsc-advances

1 Introduction

It is critically necessary to fully explore non-conventional energy sources owing to the scarcity of fossil fuels.[1] Towards this endeavour, solar cells, batteries, water splitting cells, and thermoelectric devices are considered key players.[2] The desired qualities of active ingredients for fabricating these devices include high electrical conductivity, low cost and environmental compatibility.[3] Metal sulphide nanostructures, in this regard, have received unprecedented attention because of their diverse electronic, optical, physical and chemical properties.[4] They are also used as photocatalysts, sensors and triboelectric nanogenerators (TENGs).[5] Considering all these properties, the versatility offered by copper sulfide can hardly be matched due to its availability, adaptability and low toxicity as well as its wide variety of stable and metastable phases at room temperature.[6] As a result, copper sulfide, in the nano-domain, has found numerous applications across several industries, from clean energy to biological fronts.[7–10]

Copper sulphide has various semiconducting phases with a wide range of compositions and crystal structures, including chalcocite (Cu_2S), digenite (Cu_9S_5 or $Cu_{1.8}S$), anilite (Cu_7S_4 or $Cu_{1.75}S$), roxbyite ($Cu_{58}S_{32}$ or $Cu_{1.81}S$), djurleite ($Cu_{31}S_{16}$ or $Cu_{1.94}S$), yallowite (Cu_9S_8), covellite (CuS) and villamaninite (CuS_2) (Fig. 1).[11] They are p-type narrow band gap semiconductors (1.2–2.5 eV). Possessing high absorption coefficient (10^4 cm^{-1}) and high carrier mobility, copper sulfide materials are fit for a wide variety of applications, such as photoelectrochemical cells, water splitting, photo-catalysis, thermoelectric devices and alkali ion batteries.[12–15]

Although copper sulfide in the nano-regime exhibits attractive properties and applications, the success of copper sulfide for energy and environmental remediation relies greatly on identifying affordable and scalable synthetic routes. In view of this, several methods have been adapted over the years for the synthesis of copper sulphide nanoparticles, such as solvothermal, hydrothermal, hot injection, heat up, and

[a]*Department of Chemistry, K. J. Somaiya College of Science and Commerce, Vidyavihar, Mumbai, 400077, India. E-mail: rohit.chauhan@somaiya.edu*

[b]*Chemistry Division, Bhabha Atomic Research Centre, Trombay, Mumbai, 400085, India. E-mail: tyagia@barc.gov.in*

[c]*Fuel Chemistry Division, Bhabha Atomic Research Centre, Trombay, Mumbai, 400085, India*

[d]*Technical Physics Division, Bhabha Atomic Research Centre, Trombay, Mumbai-400085, India*

[e]*Materials Science Division, Bhabha Atomic Research Centre, Trombay, Mumbai-400085, India*

† Electronic supplementary information (ESI) available. See DOI: https://doi.org/10.1039/d4ra04524f

‡ Authors contributed equally.

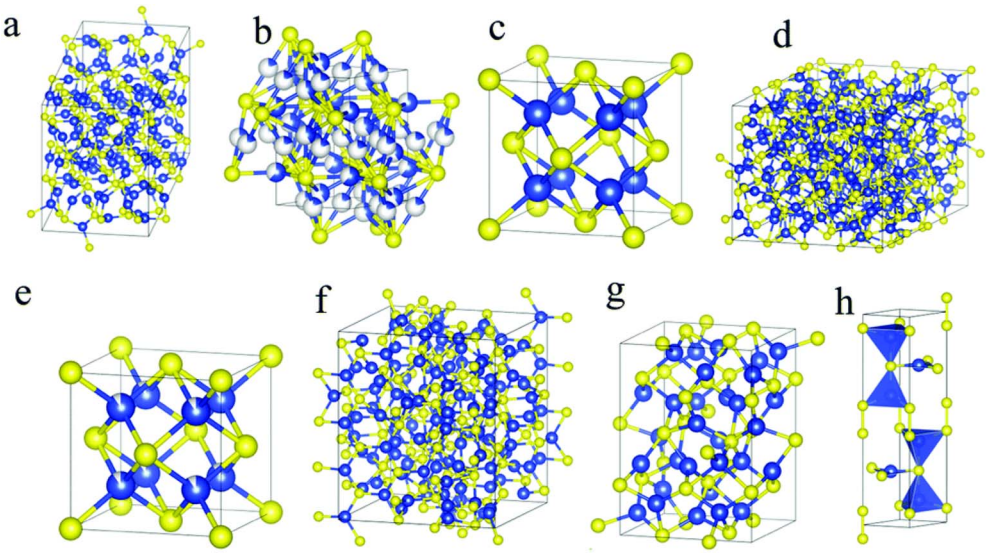

Fig. 1 Crystal structures of (a) low chalcocite, (b) high chalcocite, (c) cubic chalcocite, (d) djurleite, (e) digenite, (f) roxbyite, (g) anilite and (h) covellite phases. Blue and yellow spheres represent copper and sulfur atoms, respectively. Reproduced under Creative Common License; Copyright, RSC Publishers.[11]

sonochemical methods.[16–20] These methods generally require separate sources of copper and sulfur, commonly termed as dual source routes. However, the dual precursor route is known to produce multiple phases of copper sulfide simultaneously, thereby leading to impurities.[21] Moreover, the sulfur sources used in these techniques are hydrogen sulfide, sodium sulfide, and carbon disulfide, which are toxic and need special skill to handle. The single source molecular precursor (SSP) route has emerged as an alternative soft chemical route which, to a great extent, is able to circumvent the difficulties posed by other routes.[22] An SSP contains the desired elements within the same molecule in a bonded fashion. Due to this atomic closeness, materials from a SSP can be produced under relatively mild conditions.[23] Furthermore, SSPs are generally air and moisture stable; thus, they offer a long shelf life and materials can be synthesized from them "on-demand". SSPs are equally versatile for the fabrication of thin films. Another important aspect of SSPs is that minor modifications in the functional groups or substituents lead to effective tuning of the size, morphology, bandgap and composition of the nanostructures.[24,25] These qualities of SSPs lead to phase purity and lower defect concentration with better control over their stoichiometries with good reproducibility.

Significant efforts have been invested in developing suitable SSPs for copper sulfide nanomaterials. SSPs based on the ligand systems alkylxanthates, thiocarbamates, thiobenzoates, dithiolates, thiobiurets and dithiobiurets for the preparation of copper sulphide nanoparticles have been extensively studied. For instance, D. Yoon *et al.* synthesized $Cu_{31}S_{16}$ nanoplates in oleylamine (OAm) at 240 °C for 30 min using CuSCN as a single source precursor.[26] CuS nanocrystals were obtained by the pyrolysis of (bis(*N*-1,4-phenyl-*N*-(4-morpholinedithiocarbamato)copper(II)) complex at 900 °C for application in solar cell fabrications.[27] Chakraborty *et al.* demonstrated that the low temperature thermal breakdown of the binuclear C(I) complex $[\{(PyHS)_2CuI(PyS\}_2](OTf)_2$ leads to the formation of high quality $Cu_{1.8}S$ nanocrystals, which were further utilized as an efficient catalyst for oxygen evolution reaction (OER).[28] Catalytic and battery application of $Cu_{1.8}S$ nanocrystals synthesized from $[(PPh_3)_2CuCl(SpymMe_2)]$ are also known.[29] The photocatalytic activity of CuS nanoparticles synthesized from dithiocarbamate complex at different temperatures were studied by Ravele *et al.*[30] Mann *et al.* studied the atomic efficiency of CuS nanocrystals isolated from copper(II) bis-(2,2′-(dithiocarboxyazanediyl)diacetic acid) by hot injection technique at 90 °C in water.[31] Bis(*o*-alkylxanthato)copper(II) (alkyl = ethyl, hexyl, octyl) was used as a SSP for the synthesis of Cu_xS nanoparticles by Akhtar *et al.* In addition, the melt decomposition of ethyl and hexyl complexes afforded a mixture of digenite and covellite (CuS) and phase pure digenite, respectively; the octyl complex, on thermolysis in OAm, yielded digenite with impurities from the djurleite ($Cu_{31}S_{16}$) phase.[32]

Our group is actively involved in designing and synthesizing new metal complexes featuring internally functionalized hemilabile ligands. The rich chemistry of these ligands with a variety of metal ions[33] prompted us to utilize these complexes as efficient SSPs for metal chalcogenide nanomaterials and thin films. With our continued interest in the field, in the present study, we identified two potential copper thiolate complexes, namely $CuX(dmpymSH)(PPh_3)_2$ (X = Cl, I). These complexes have been previously reported by our group for their catalytic activity. In the current study, the aim is to explore the prospect of these known compounds as efficient SSPs for copper sulfide nanomaterials. Interestingly, the investigation shows that, depending upon the halogen substitution in the complex, phase pure djurleite ($Cu_{31}S_{16}$) and digenite (Cu_9S_5) nanoparticles can be synthesized. Of these, djurleite, being low temperature phase, has rarely been isolated though a precursor route. The

photoelectrochemical cell (PEC) studies based on these nanomaterials suggest their potential as promising materials for solar cell applications.

2 Experimental

2.1 Chemicals

All the chemicals used during the reaction were purchased from TCI chemicals and used without purification. The ligands 4,6-dimethyl pyrimidine thiol,[34] $[CuCl(PPh_3)_2]$ and $[CuIPPh_3]_4$ (ref. 35) were prepared according to reported literature methods.

2.2 Instrumentation

The ^1H, $^{13}C\{^1H\}$ and $^{31}P\{^1H\}$ NMR spectra of the complexes were obtained on a Brucker Advance-II 500, 125 and 202.4 MHz spectrometer. For ^1H NMR and $^{13}C\{^1H\}$ NMR, $CDCl_3$ was used as an internal reference solvent with resonances at 7.26 ppm and 77.16 ppm; $^{31}P\{^1H\}$ NMR was studied using 85% H_3PO_4 as an external standard. The IR spectra of complexes were recorded on a PerkinElmer 577 FTIR model spectrophotometer operating over the range of 400–4000 cm^{-1} using the KBr pellet method. Thermogravimetric analyses (TGA) were carried out using a Nitzsch STA 409 PC-Luxx TG-DTA instrument that was calibrated with $CaC_2O_4 \cdot H_2O$. The TG curves were recorded at a heating rate of 10 °C min^{-1} under a flow of argon. The X-ray powder diffraction patterns were obtained using a Philips PW-1820 diffractometer using Cu-K_α radiation. For XPS analysis, a film was prepared by drop coating the sample on a glass substrate and drying under an IR lamp. The binding energy scale in XPS was calibrated to the C 1s line of 284.5 eV. All the deconvolutions and fittings were done using CasaXPS software. Optical diffuse reflectance measurements in the range of 200–1100 nm (1.12 eV to 6.2 eV) were performed using a JASCO V-670 two-beam spectrometer with a diffuse reflectance (DR) attachment consisting of an integration sphere coated with $BaSO_4$ which was used as the reference material. The measured reflectance data were converted to absorption (A) using the Kubelka–Munk remission function. The band gaps of the samples were estimated by extrapolating the linear portion of the plot to the X (energy) axis. SEM and EDS measurements were carried out using the ULTRA 55 FESEM of Zeiss and Oxford Inca instruments, respectively. A Zeiss Libra 200 FE transmission electron microscope (TEM) operating at an accelerating voltage of 200 kV was used for TEM studies. The samples for TEM were prepared by placing a drop of sample dispersed in acetone/toluene on a carbon coated copper grid.

2.3 Synthesis of $[CuCl(dmpymSH)(PPh_3)_2]$ (1)

The complex $[CuCl(dmpymSH)(PPh_3)_2]$ was synthesized according to the literature method.[36] 4,6-dimethyl pyrimidine-2-thiol·HCl (dmpymSH·HCl) (56 mg, 0.40 mmol) was dissolved in methanol (10 mL) and was added to a solution of $[CuCl(PPh_3)_2]$ (249 mg, 0.40 mmol) in acetonitrile (20 mL) under an inert atmosphere. The reaction mixture was stirred for 6 hours at room temperature. The resulting solution was evaporated under reduced pressure. About 5 mL of product was precipitated in diethyl ether to obtain a yellow powder which was thoroughly washed with hexane and diethyl ether. The powder was dissolved in acetonitrile solution and the resultant solution under cryogenic conditions afforded yellow crystals of the compound. (Yield: 248 mg, 63.4%; m.p. = 110 °C (dec.)). Anal. Calcd. for $C_{42}H_{38}N_2ClP_2SCu$ (%): C, 66.04; H, 5.01; N, 3.66; S, 4.19; Found: C, 65.60; H, 4.98; N, 3.51; S, 4.02%. IR (KBr, cm^{-1}): 496 (m), 688 (m), 749 (m), 840 (m), 1036 (m), 1252 (s), 1433 (s), 1476 (s), 2948 (w) (Fig. S1†). ^1H NMR (500 MHz, $CDCl_3$) δ: 2.41 (s, 3H, Me), 2.27 (s, 3H, Me), 6.63 (s, 1H C_3HN_2), 7.19–7.15 (m, 12H, Ph), 7.23 (m, 6H, Ph), 7.39–7.33 (m, 12H, Ph); $^{13}C\{^1H\}$ NMR (125 MHz, $CDCl_3$): δ 23.69, 115.2, 139.0, 176.4 ppm; $^{31}P\{^1H\}$ NMR (202.4 MHz, $CDCl_3$) δ: −3.71 ppm (Fig. S2–S4†).

2.4 Synthesis of $[CuI(dmpymSH)(PPh_3)_2]$ (2)

The complex $[CuI(dmpymSH)(PPh_3)_2]$ was prepared in a similar fashion to **1** using dmpymSH·HCl (81 mg, 0.58 mmol) and $[CuI(PPh_3)]_4$ (259 mg, 0.143 mmol) to afford a yellow powder of the compound (Yield: 96 mg, 59.7%; m.p. = 170 °C (dec)). Anal. Calcd. for $C_{42}H_{38}N_2SIP_2Cu$ (%): C, 58.98; H, 4.47; N, 3.27; S, 3.74; Found: C, 58.94; H, 4.64; N, 3.21; S, 3.69%. IR (KBr, cm^{-1}): 502 (s), 545 (m), 693 (w), 693 (s), 749 (s), 1032 (m), 1251 (m), 1438 (m), 1476 (s), 1581 (m), 3047 (s) (Fig. S5†). ^1H NMR (500 MHz, $CDCl_3$) δ: 2.32 (s, 3H, Me), 2.28 (s, 3H, Me), 6.65 (s, 1H, $C_4H(4,6\text{-}Me_2)$), 7.37–7.30 (m, 12H, Ph), 7.40–7.38 (m, 6H, Ph), 7.44–7.41 (m, 12H, Ph); $^{13}C\{^1H\}$ NMR (125 MHz, $CDCl_3$): δ 23.69 ppm, 115.24, 139.03, 162.23; $^{31}P\{^1H\}$ NMR (202.4 MHz, $CDCl_3$) δ: −4.75 ppm (Fig. S6–S8†).

2.5 Synthesis of Cu_9S_5 and $Cu_{31}S_{16}$ nanoparticles

Copper sulfide nanostructures were synthesized by the thermolysis of complexes **1** and **2** as molecular precursors in OAm using the hot-injection method. In a typical hot-injection process, 8 mL of high boiling solvent (OAm) along with required amount of the precursor were taken in a three-necked round bottom flask and degassed at 120 °C under a constant flow of Ar for 30 min to remove any unwanted moisture. Subsequently, the temperature was elevated to the required decomposition temperature and a suspension of the respective precursor in 2 mL of OAm was swiftly injected into the hot solvent and the reaction was continued for 10 minutes. Then, the reaction mixture was cooled to ∼70 °C and 5 mL methanol was injected for complete precipitation of the desired copper sulfide nanostructures. The synthesized material was collected after repeated washing and centrifugation to remove excess capping agent. The final product was collected as black residue.

2.6 Photo-switching experiment

The photo-switching measurements of the synthesized materials were carried out in an aerobic atmosphere by fabricating two separate prototype photo electrochemical cells (PEC) constructed using silicon wafers coated with the synthesized Cu_9S_5 and $Cu_{31}S_{16}$ nanostructures as the working electrodes and platinum plate and platinum wire as the counter and pseudo reference electrodes, respectively. An aqueous electrolyte of composition Na_2S (0.6 M) : Na_2SO_3 (0.8 M) (1 : 2) was employed

in the cell. Two working electrodes were prepared by spin coating a colloidal solution of the as prepared nanostructures in chloroform on the rough surface of n-type Si wafers (1 cm × 1 cm) of (1 0 0) orientation and a thickness of 300 μm. The film was annealed at 150 °C for 1 h. A 36 W fluorescent white light with less than 3% UV content was used as light source. The light intensity at the effective area of the cell ($S = 0.785$ cm^2) was 200 μW cm^{-2}.

3 Results and discussion

3.1 Synthesis and characterization of the complexes [CuCl(dmpymSH)(PPh$_3$)$_2$] (1) and [CuI(dmpymSH)(PPh$_3$)$_2$] (2)

tTreatment of one equivalent of sodium salt of the ligand 4,6-dimethyl-2-pyrimidylthiol·HCl (dmpymSH·HCl) with the Cu-PPh$_3$ complex [CuCl(PPh$_3$)$_2$] in acetonitrile afforded desired complex [CuCl(dmpymSH)(PPh$_3$)$_2$] (**1**). Reaction of four equivalents of the same ligand with the tetranuclear mono-iodo analogue of the Cu-PPh$_3$ analogue [CuI(PPh$_3$)]$_4$ yielded 4 moles of the complex [CuI(dmpymSH)(PPh$_3$)$_2$] (**2**) as summarized in Scheme 1 and the molecular structure of **1** is depicted in Fig. 2.

Since the metal–organic complexes under study are potential SSPs for the synthesis of copper sulfide material, thermal analyses of the former become indispensable. The decomposition behavior of the complexes under thermal agitation and the characterization of the residue provide valuable insights about their viability as SSPs. Thus, thermogravimetric analysis (TG) was carried out and the corresponding TG curves are presented in Fig. S9.† From the TG curves of **1** and **2**, it can be seen that the complexes are thermally stable up to ∼180 °C. Beyond this temperature, they undergo clean, single step decompositions. The observed ∼80.48% weight loss for **1** signifies the formation of $Cu_{1.8}S$ (calculated weight loss for conversion of **1** to $Cu_{1.8}S$ 80.81%). The weight loss (∼89%) for **2**, on the other hand, can be matched with the calculated weight loss from **2** to CuS (calculated weight loss ∼88.8%). This suggests that both the complexes, with proper choice of decomposition environment, can serve as efficient single source molecular precursors for generating copper sulfide nanostructures.

3.2 Preparation and characterization of copper sulfide nanomaterials

From the decomposition signature of the title complexes observed in the TG analysis, it can be gathered that both [CuCl(dmpymSH)(PPh$_3$)$_2$] (**1**) and [CuI(dmpymSH)(PPh$_3$)$_2$] (**2**) can serve as suitable SSPs for the preparation of copper sulfide materials. The SSPs were chosen because the metal center is attached to different halogen atoms (–Cl and –I). Since –I is larger in size and a better leaving group compared to –Cl, the thermal decomposition behavior of the aforementioned complexes might differ in solvents with electron donating ability. Additionally, the thermolysis of these two complexes also provides a fair chance to isolate different phases of copper sulfide. There are several reports where the effects of different alkyl/aryl or various other functionalities in SSP have been studied for their effect on the final material. However, it will be interesting to see the effect of the halogen attached to the metal center in an SSP on the course of material production, as reports on this are scarce in the literature. To further ascertain these postulates, thermolysis of the SSPs was performed by hot injection method in OAm for 10 minutes. OAm is a versatile solvent, widely used for nanomaterial synthesis. The popularity of OAm for nanomaterial synthesis is due to the fact that it serves as both capping agent and high boiling solvent.[37] Another advantage of OAm is that it significantly lowers the thermolysis temperature of SSPs compared to solid state decomposition, thereby serving as a catalyst.[38] The temperature was set at the minimum temperature where the respective complexes show a decomposition signature. Complex **1** showed signs of decomposition at 220 °C, and thus that temperature was maintained for 10 minutes. In contrast, complex **2**

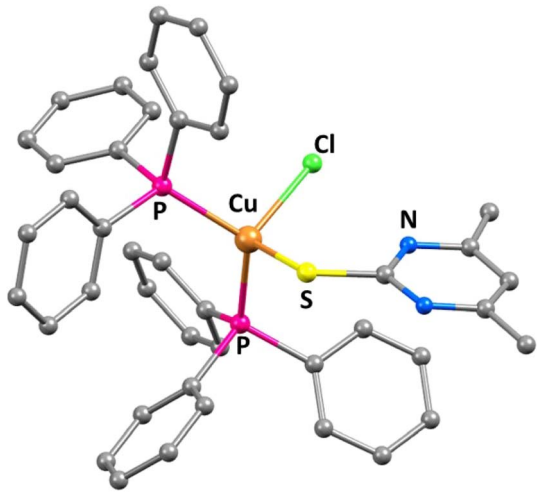

Fig. 2 Molecular structure of [CuCl(dmpymSH)(PPh$_3$)$_2$] (**1**). Reproduced from CCDC No. 2210066.

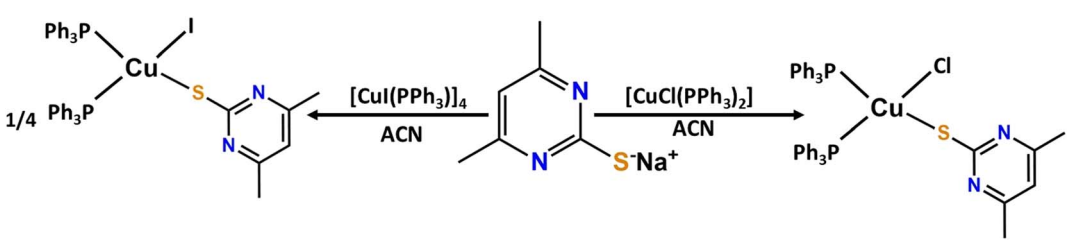

Scheme 1 Synthesis of [CuCl(dmpymSH)(PPh$_3$)$_2$] (**1**) and [CuI(dmpymSH)(PPh$_3$)$_2$] (**2**).

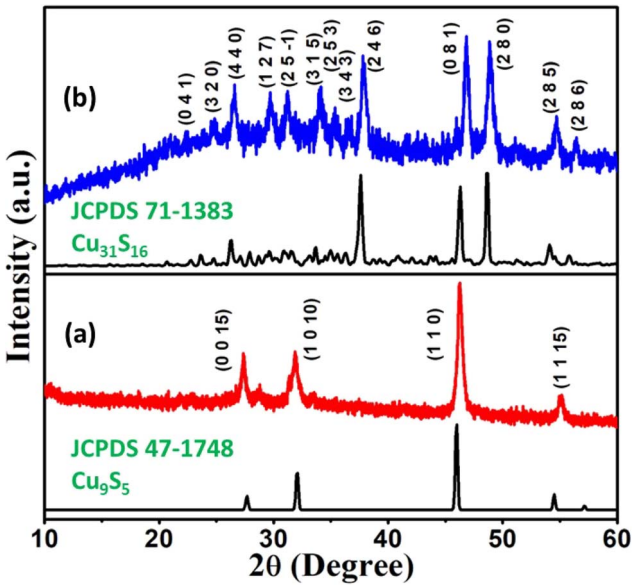

Fig. 3 XRD profiles of copper sulfide nanostructures obtained *via* the thermolysis of (a) [CuCl(dmpymSH)(PPh_3)$_2$] (**1**) and (b) [CuI(dmpymSH)(PPh_3)$_2$] (**2**).

exhibited a peculiar behaviour. It underwent breakdown to produce a brown precipitate at only 95 °C, and the reaction was continued for same duration. Repeat thermolysis experiments exhibited negligible deviation from the abovementioned reaction conditions, which proves the high reproducibility of nanomaterial production *via* these SSPs.

The primary characterization of the decomposed products' phase purities and crystal structures was done by PXRD studies. The PXRD patterns of the products are presented in Fig. 3. Four prominent reflections can be observed in the case of the material synthesized from **1** at $2\theta = 28.0$, 32.4, 42.6 and 55.1°. These peaks can be assigned to the reflections originating from the (0 0 15), (1 0 10), (110) and (1 1 15) planes of rhombohedral Cu_9S_5 (digenite) (JCPDS Card No 47-1748). Interestingly, the PXRD pattern of the powder yielded from **2** features reflections that can be matched exactly with those emanating from the planes of phase pure $Cu_{31}S_{16}$ (djurleite) (JCPDS Card No 47-1748) material. In both cases, the FWHM of the peaks suggest the formation of nanosized particles. The isolation of the Cu_9S_5 phase is observed, as, according to the Cu–S system phase diagram,[39] digenite is one of the most stable phases of copper

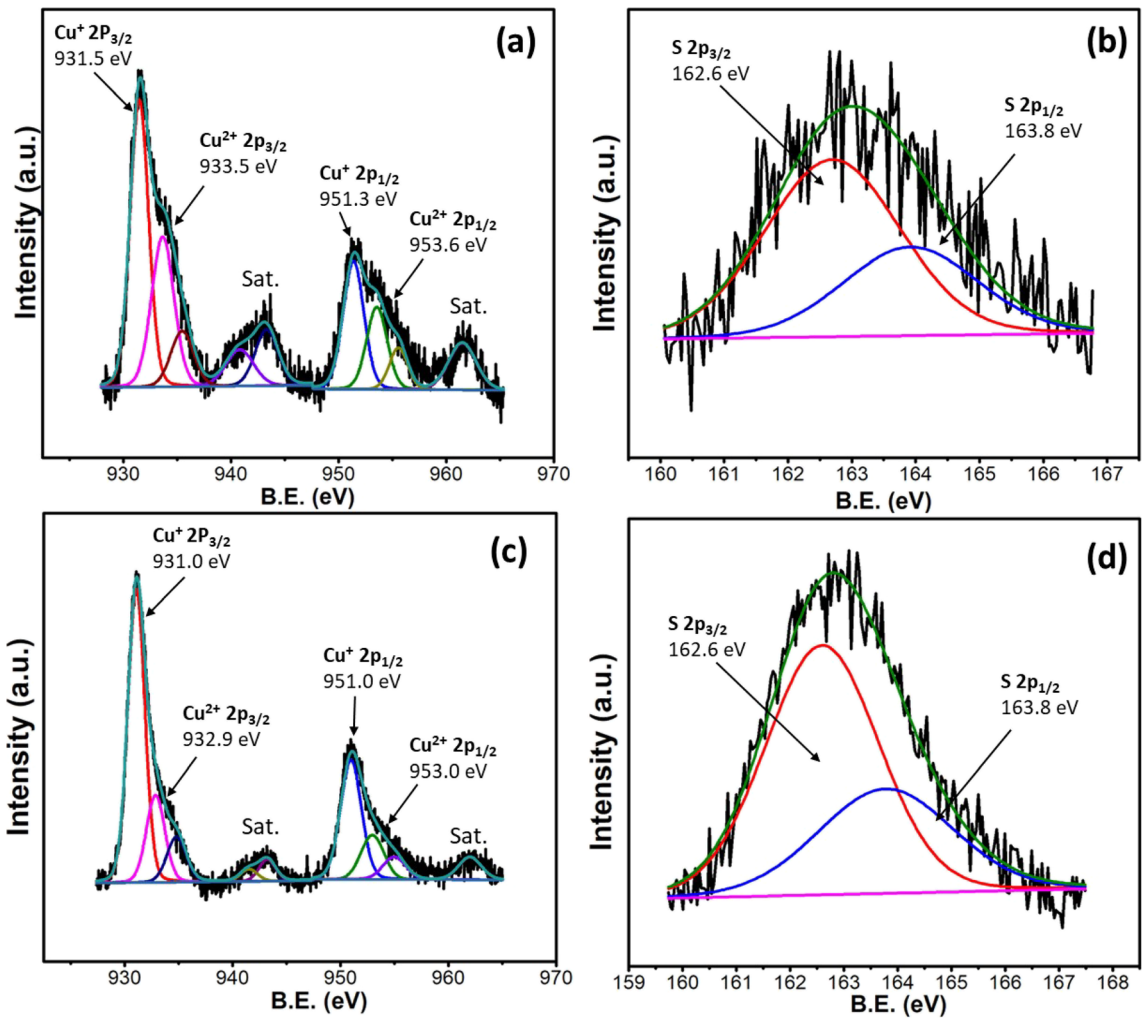

Fig. 4 Cu2p and S2p XPS spectra for (a and b) Cu_9S_5 and (c and d) $Cu_{31}S_{16}$ nanostructures.

sulfide. However, the production of the metastable $Cu_{31}S_{16}$ phase was intriguing to us, as reports on the synthesis of this phase though an SSP are rare in open publications.[40] A detailed literature survey revealed that the djurleite phase is only stable up to 95 ± 3 °C at atmospheric pressure.[41–43] Thus, the primary reason behind its formation *via* SSP **2** is the lower than boiling water decomposition temperature of the complex in OAm. However, an explanation was still required regarding the ultralow decomposition temperature of **2** compared to **1**. It is important to mention here that the decomposition of an SSP and the subsequent production of the respective material is a complex process. Although the decomposition pathways for xanthate and some selected dithiocarbamate complexes are known,[37] they remain elusive for most of the complexes. A plausible explanation in the present case can be given based on the weak nature of the Cu–I bond in **2** compared to the Cu–Cl in **1**. Due to the better leaving property of iodide, complex **2** undergoes fast low-temperature rupture of the metal–halogen linkage in presence of OAm, which is an electron rich solvent. Once the Cu–I bond is split, the complex cascade process involved in the decomposition mechanism is accelerated and completes at 95 °C due to the added catalytic aid from OAm. As a result, the djurleite phase in pure form was isolated. The average crystallite sizes of the Cu_9S_5 and $Cu_{31}S_{16}$ nanostructures calculated from the Scherrer equation were found to be 23 and 16 nm, respectively.

The copper sulfide nanostructures were further characterized by XPS analysis for an in-depth understanding of their purities and oxidation states. The Cu2p XPS spectra of the Cu_9S_5 and $Cu_{31}S_{16}$ synthesized from **1** and **2**, respectively, are presented in Fig. 4a and c. The spectra reveal splitting due to the presence of both Cu^+ and Cu^{2+} ions. This corroborates the mixed valence nature of both Cu_9S_5 and $Cu_{31}S_{16}$. These peak positions are consistent with those reported in literature for metal rich copper sulfide material.[44] The presence of paramagnetic Cu^{2+} is reflected in the prominent satellite peaks.[45] The XPS spectra of sulfur in both cases (Fig. 4b and d) divulge $S2p_{3/2}$ and $S2p_{1/2}$ peaks. This confirms the presence of only one sulfur species in both samples, corresponding to the existence of S^{2-}. These findings are in agreement with literature values for copper sulfide materials.[46,47]

For better insight into the compositions of the synthesized copper sulfide nanostructures, EDS was performed (Fig. S11†). The study revealed that the atom percent ratios of Cu : S are 64.3 : 35.7 (1.8 : 1) and 65.9 : 34.1 (1.93 : 1) for the materials synthesized from **1** and **2** in OAm, respectively, corroborating that phase pure digenite and djurleite were obtained from the respective SSPs. The 2-D elemental mapping of the samples (Fig. S12†) confirms the uniform distribution of the constituent elements within the nanostructures.

The morphologies of the as synthesized nanoparticles were investigated by electron microscopy. The scanning electron microscopy (SEM) images of the Cu_9S_5 and $Cu_{31}S_{16}$ nanostructures (Fig. 5a and b) obtained from **1** and **2** divulge the presence of nanoflakes and nearly spherical particles. The bright field TEM images (Fig. 5c and d) of the materials support these morphological findings. The HRTEM images (Fig. 5e and f) present distances of 2.0 and 3.38 Å between the lattice fringes, which can be indexed to the (110) and (004) planes of the Cu_9S_5 and $Cu_{31}S_{16}$ materials.

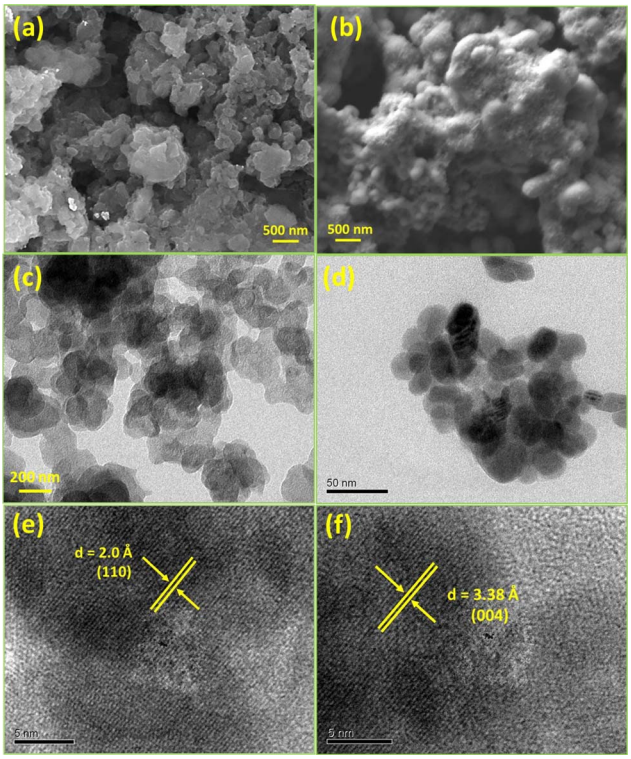

Fig. 5 (a and b) SEM, (c and d) TEM and (e and f) HRTEM images of Cu_9S_5 and $Cu_{31}S_{16}$ nanoparticles.

3.3 Optical properties

Copper sulfides are undoubtably one of the better materials for green energy applications including photovoltaic devices, photocatalysis, sensors, thermoelectric devices and alkali ion batteries.[47–49] Tunable and narrow direct band-gap energies in the range of 1.2–2.0 eV are the prime factor which posit them as appealing materials for energy and environmental remedy.[50,51] Having an optimal band gap is a prerequisite for these materials to be used in photoelectrochemical devices. With this viewpoint, the optical properties of the as synthesized Cu_9S_5 and $Cu_{31}S_{16}$ nanoparticles were determined by diffuse reflectance spectroscopy (DRS) and the optical band gaps of these materials were calculated using a plot of the Kubelka–Munk function, $F(R)$, as given in the equation

$$[F(R)h\nu]^n = A(h\nu - E_g)$$

where $h\nu$ is photon energy, A is a constant, E_g denotes the band gap, and n depends on the nature of the optical transition.

The direct band gap of the materials was calculated using Tauc's model ($n = 2$) as represented in Fig. 6. The plot shows that the direct optical band gaps for the digenite (Cu_9S_5) and djurleite ($Cu_{31}S_{16}$) nanostructures are 2.25 and 2.40 eV, respectively. It is to be noted that these values are blue shifted compared to the bulk band gap values of the respective

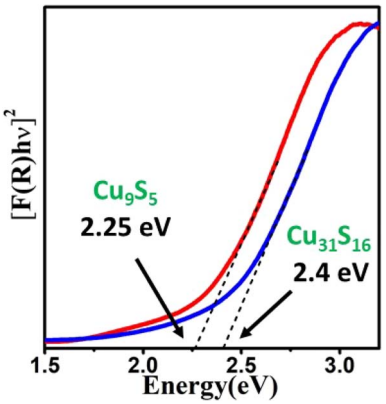

Fig. 6 Plots of $[F(R)h\nu]^2$ *vs.* energy (eV) generated by Kubelka–Munk transformation of solid-state diffuse reflectance data of Cu_9S_5 and $Cu_{31}S_{16}$ nanoparticles.

materials (E_g = 1.5 eV and 1.8 eV for bulk Cu_9S_5 and $Cu_{31}S_{16}$).[51,52] There are several probable causes which impart blue shift to the band gap of nanoparticles. These include lattice distortions, surface lattice defects, quantum confinement, and the surface effect of the carriers.[53] The quantum confinement effect, however, only occurs in nanocrystals smaller than the corresponding exciton Bohr radii. For Cu_9S_5 and $Cu_{31}S_{16}$, unfortunately, there are no reports which clearly state the values of the Bohr radii. However, a fair idea of them can be obtained from a study by Burda and co-workers. According to the study, the excitonic Bohr radii for $Cu_{2-x}S$ type materials are in the range of 10–15 nm.[54] Since the average crystallite sizes of all the synthesized nanostructures in the current study are larger than the corresponding Bohr radii, the involvement of the quantum confinement effect is debatable and the observed blue shifts may be attributed to either lattice distortion or surface lattice defects. The optical properties observed here are comparable to the literature values. These band gap values indicate that the as prepared materials possess good electronic conductivity and can be utilized as a suitable absorber layer in photo-electrochemical cells.

3.4 Photo-switching characteristics of Si/Cu_9S_5 and Si/$Cu_{31}S_{16}$ based liquid junction photoelectrochemical cells

Cu_9S_5 (digenite) and $Cu_{31}S_{16}$ (djurleite) are p-type semiconductors and are considered metal deficient compared to Cu_2S (chalcocite). The Cu deficiency in these materials

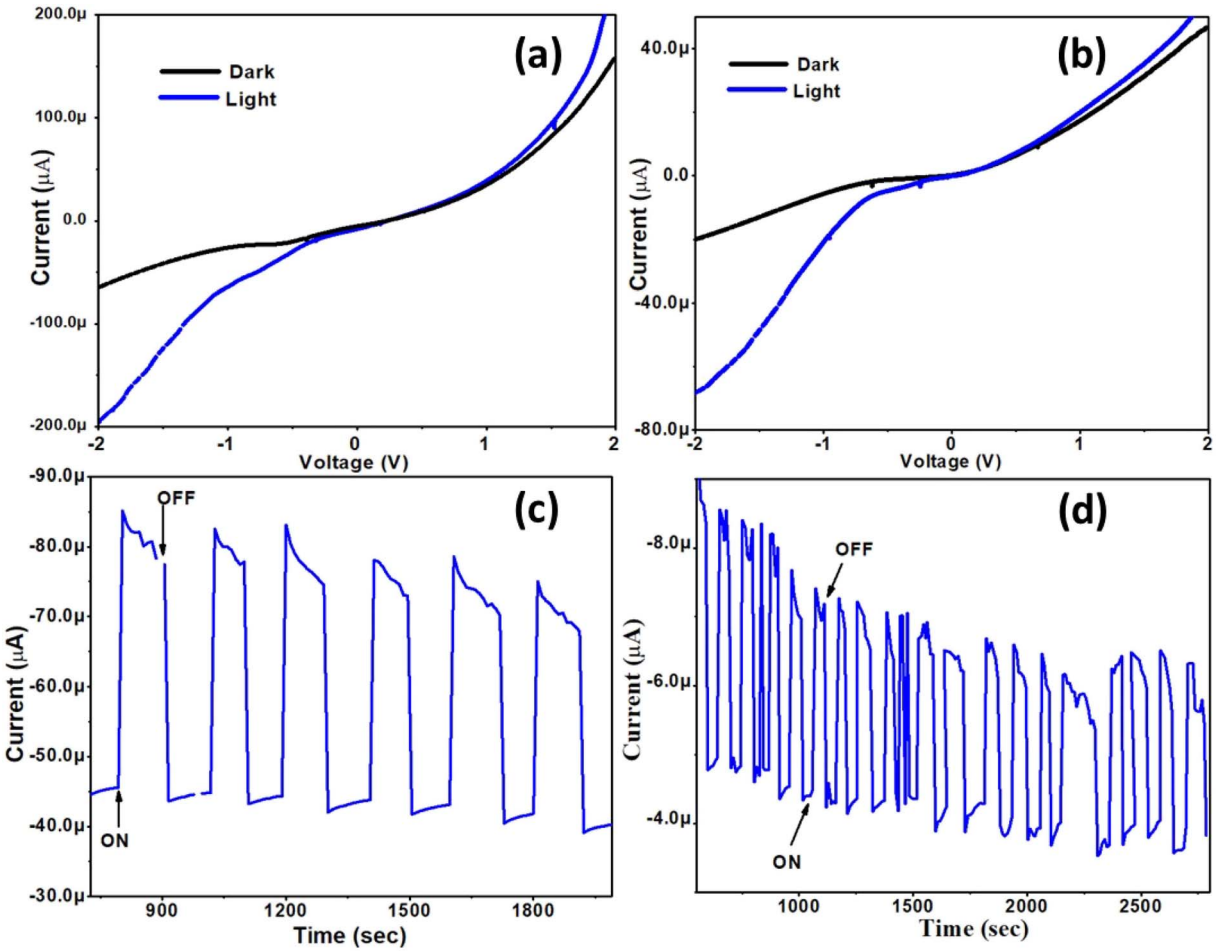

Fig. 7 (a and b) *I–V* characteristics and (c and d) switching behaviour under alternating light and dark conditions for Cu_9S_5 and $Cu_{31}S_{16}$ nanoparticles.

generates free holes which act as carriers. Thus, the electrochemistry of these materials is quite rich. Kundu *et al.*, in a recent investigation, achieved tailoring of the electrochemical behavior of mixed valent copper sulfide nanomaterials during water electrolysis.[55] They also correlated the device performance to the atomic arrangements and coordination geometry of the surface exposed sites. Liu *et al.* studied these Cu vacancies within the crystal lattices of metal deficient copper sulfides and concluded that the phenomenon enhances their performance in photodetectors or solar cells.[56] These facts prompted us to apply the as-synthesized copper sulfides as photon absorber materials and evaluate their photo response. Two prototype photo electro-chemical cells in a three electrode system were fabricated. The working electrode was fabricated by spin coating Cu_9S_5 or $Cu_{31}S_{16}$ nanoparticles over a Si substrate followed by evaporation of the solvent. The photo response of the $Si/Cu_{1.8}S$ working electrode as a function of time was measured under a light intensity of 200 μW cm^{-2} with a bias voltage of −1.5 V in the three electrode photoelectrochemical setup. The photo-switching characteristics of the pristine Cu_9S_5 and $Cu_{31}S_{16}$ nanoparticles are given in Fig. 7a and b, respectively. In both cases, the *I–V* curves display nonlinear behaviour with an increase in current under illumination conditions due to photogenerated carriers. The consistent switching characteristics of the samples during the repeated light ON–OFF experiments suggest good photosensitivity, while the reproducibility of the current suggests high stability of the nanostructures under alternating light and dark conditions. The results indicate the potential application of Cu_9S_5 and $Cu_{31}S_{16}$ nanoparticles in photo detector and photovoltaic applications.[57]

4 Conclusions

The present study deals with the application of copper complexes with hemilabile pyrimidyl thiolate ligand as potential precursors for the production of copper sulfide nanomaterials. Two complexes featuring different halogen substitution at the central Cu atom, namely $CuX(dmpymSH)(PPh_3)_2$ (where X = Cl, I), were synthesized. Thermal breakdown of these complexes in OAm resulted in the formation of phase pure Cu_9S_5 (digenite) and $Cu_{31}S_{16}$ (djurleite) nanomaterials with high reproducibility. The superior leaving property of –I facilitated the low-temperature thermolysis of the latter complex, leading to the stabilization of the djurleite phase, a low-temperature form of copper sulfide. Characterization revealed that the digenite nanoparticles were comprised of nanoflakes while nearly spherical particles were evident in the djurleite nanoparticles. The optical studies on the as-synthesized materials revealed band gaps in the range of 2.25–2.4 eV, which is optimum for their potential application as efficient absorber materials in solar cells. The pristine nanomaterial-based PEC devices exhibited stable photo-switching characteristics with good photocurrent generation under an alternating light and dark environment. Altogether, this report presents a facile and scalable route to access digenite and djurleite nanostructures by simple precursor engineering. The authors believe that this report will add great value to the library of SSPs coinage metal chalcogenides for real-life applications.

Data availability

The data supporting this article have been included as part of ESI.†

Conflicts of interest

The authors declare no conflicts of interest.

Acknowledgements

We thank Dr N. Choudhury, Head, Chemistry Division, Bhabha Atomic Research Centre for the encouragement of this work.

References

1 L. Wang, Y. Lu, J. Liu, M. Xu, J. Cheng, D. Zhang and J. B. Goodenough, *Angew. Chem., Int. Ed.*, 2013, **52**, 1964–1967.
2 Z. Yu, Q. Zhou, J. Zhu, Q. Yan, S. X. Dou and W. Sun, *Adv. Funct. Mater.*, 2017, **27**, 1702317.
3 Y. Zhang, L. Zhang, T. Lv, P. K. Chu and K. Huo, *ChemSusChem*, 2020, **13**, 1–42.
4 L. Wen, Q. Chen, L. Zhou, M. Huang, J. Lu, X. Zhong and Y. Ou, *Opt. Mater.*, 2020, **108**, 110172.
5 Z. Shao, J. Chen, Q. Xie and L. Mi, *Coord. Chem. Rev.*, 2023, **486**, 215118.
6 J. H. Yoo, M. Ji, J. H. Kim, C. H. Ryu and Y. I. Lee, *J. Photochem. Photobiol., A*, 2020, **401**, 112782.
7 L. Su, Y. Hu, Z. Ma, L. Miao, J. Zhou, Y. Ning and J. Qian, *Sol. Energy Mater. Sol. Cells*, 2020, **210**, 110484.
8 M. Tanveer, C. Cao, I. Aslam, Z. Ali, F. Idrees, W. S. Khan, M. Tahir, S. Khalid, G. Nabi and A. Mahmood, *New J. Chem.*, 2015, **39**, 1459–1468.
9 M. A. Kamyabi and M. Moharramnezhad, *Microchem. J.*, 2022, **179**, 107421.
10 X. Yan, Y. Gu, C. Li, B. Zheng, Y. Li, T. Zhang and M. Yang, *Anal. Methods*, 2018, **10**, 381–388.
11 L. Chen, H. Hu, Y. Chen, J. Gao and G. Li, *Mater. Adv.*, 2021, **2**, 907–926.
12 M. Ye, X. Wen, N. Zhang, W. Guo, X. Liu and C. Lin, *J. Mater. Chem. A*, 2015, **3**, 9595–9600.
13 Z. H. Ge, Y. H. Zhang, D. Song, X. Chong, P. Qin, F. Zheng, J. Feng and L. D. Zhao, *J. Mater. Chem. A*, 2018, **6**, 14440–14448.
14 M. Balaz, A. Augustyniak, B. Tatykayev, Z. Shalabayev, G. Burashev, E. Dutkova, N. Daneu, J. Briancin, L. Balazova, L. Tkacikova, M. Stahorsky, M. Achimovicova and P. Balaz, *Faraday Discuss.*, 2023, **241**, 367–386.
15 Q. Liu, K. Xiao, L. Wen, Y. Dong, G. Xie, Z. Zhang, Z. Bo and L. Jiang, *ACS Nano*, 2014, **8**, 12292–12299.
16 A. Ghezelbash and B. A. Korgel, *Langmuir*, 2005, **21**, 9451–9456.
17 Q. Lu, F. Gao and D. Zhao, *Nano Lett.*, 2002, **2**, 725–728.

18 Y. C. Zhang, T. Qiao and X. Y. Hu, *J. Cryst. Growth*, 2004, **268**, 64–70.
19 S. Gorai, D. Ganguli and S. Chaudhuri, *Cryst. Growth Des.*, 2005, **5**, 875–877.
20 P. L. Saldanha, R. Brescia, M. Prato, H. Li, M. Povia, L. Manna and V. Lesnyak, *Chem. Mater.*, 2014, **26**, 1442–1449.
21 V. Brune, M. Grosch, R. Weibing, F. Hartle, M. Frank, S. Mishra and S. Mathur, *Dalton Trans.*, 2021, **50**, 12365–12385.
22 G. Karmakar, A. Y. Shah, A. Tyagi, A. P. Wadawale, G. Kedarnath, N. N. Kumar and J. Bahadur, *New J. Chem.*, 2022, **46**, 3871–3881.
23 S. Mishra, *Chem. Commun.*, 2022, **58**, 10136–10153.
24 S. Razzaque, M. D. Khan, M. Aamir, M. Sohail, S. Bhoyate, R. K. Gupta, M. Sher, J. Akhtar and N. Revaprasadu, *Inorg. Chem.*, 2021, **60**, 1449–1461.
25 N. Revaprasadu, M. A. Malik and P. O'Bien, *S. Afr. J. Chem.*, 2004, **57**, 40–43.
26 D. Yoon, H. Jin, S. Ryu, S. Park, H. Baik, S. J. Oh and K. Lee, *CrystEngComm*, 2015, **17**, 4627–4631.
27 B. Chakraborty, S. Kalra, R. Beltrán-Suito, C. Das, T. Hellmann, P. W. Menezes and M. Driess, *Chem.–Asian J.*, 2020, **15**, 852–859.
28 M. A. Agoro, E. L. Meyer, J. Z. Mbese and K. Manu, *Catalysts*, 2020, **10**, 300.
29 G. Karmakar, A. Tyagi, K. K. Halankar, S. Nigam, B. P. Mandal, A. Wadawale, G. Kedarnath and A. Debnath, *Dalton Trans.*, 2023, **52**, 1461–1475.
30 M. P. Ravele, O. A. Oyewo and D. C. Onwudiwe, *Catalysts*, 2021, **11**, 899.
31 P. B. Mann, I. J. McGregor, S. Bourke, M. Burkitt-Gray, S. Fairclough, M. T. Ma and M. Green, *Nanoscale Adv.*, 2019, **1**, 522–526.
32 M. Akhtar, Y. Alghamdi, J. Akhtar, Z. Aslam, N. Revaprasadu and M. A. Malik, *Mater. Chem. Phys.*, 2016, **180**, 404–412.
33 P. Halder, S. Ghorai, S. Banerjee, B. Mondal and A. Rana, *Dalton Trans.*, 2017, **46**, 13739–13744.
34 C. Costa, E. Reisenhofer, L. Stefani and J. Znorg, *Nucl. Chem.*, 1965, **27**, 2581–2584.
35 S. P. Yadav, D. Sahil, R. S. Chauhan, R. J. Butcher, A. Tyagi, G. Karmakar and C. Dash, *ChemistrySelect*, 2024, **9**, e202303058.
36 G. Karmakar, A. Tyagi and A. Y. Shah, *Coord. Chem. Rev.*, 2024, **504**, 215665.
37 M. D. Khan, M. Aamir, G. Murtaza, M. A. Malik and N. Revaprasadu, *Dalton Trans.*, 2018, **47**, 10025–10034.
38 D. J. Chakrabarti and D. E. Laughlin, *Bull. Alloy Phase Diagrams*, 1983, **4**, 254–271.
39 X. Chen, J. Yang, T. Wu, L. Li, W. Luo, W. Jiang and L. Wang, *Nanoscale*, 2018, **10**, 15130–15163.
40 M. Pósfai and P. R. Buseck, *Am. Min.*, 1994, **79**, 308–315.
41 K. Szopa, T. Krzykawski, K. Banasik, P. Król, S. Skreczko, S. A. Mounteanou and M. Koziarska, *Minerals*, 2021, **11**, 454.
42 B. J. Mulder, *Cryst. Res. Technol.*, 1973, **8**, 825–832.
43 L.-N. Qiao, H.-C. Wang, Y. Shen, Y.-H. Lin and C.-W. Nan, *Nanomaterials*, 2017, **7**, 19.
44 S. C. Riha, D. C. Johnson and A. L. Prieto, *J. Am. Chem. Soc.*, 2011, **133**, 1383–1390.
45 J. Chen, Z. Qin and D. W. Shoesmith, *J. Electrochem. Soc.*, 2010, **157**, C338–C345.
46 J. Zhou, G. Tian, Y. Chen, Y. Shi, C. Tian, K. Pan and H. Fu, *Sci. Rep.*, 2014, **4**, 4027.
47 G. Karmakar, A. Tyagi, K. K. Halankar, S. Nigam, B. P. Mandal, A. Wadawale, G. Kedarnath and A. Debnath, *Dalton Trans.*, 2023, **52**, 1461–1475.
48 G. Karmakar, A. Y. Shah, M. Kumar, V. Singh, G. K. Kole and A. Tyagi, *J. Mol. Struct.*, 2024, **1295**, 136707.
49 Y.-X. Zhang, J. Feng and Z.-H. Ge, *Chem. Eng. J.*, 2022, **428**, 131153.
50 Y. Wu, C. Wadia, W. Ma, B. Sadtler and A. P. Alivisatos, *Nano Lett.*, 2008, **8**, 2551–2555.
51 T. Kuzuya, Y. Tai, S. Yamamuro and K. Sumiyama, *Sci. Technol. Adv. Mater.*, 2005, **6**, 84–90.
52 A. C. Rastogi and S. Salkalachen, *Thin Solid Films*, 1982, **97**, 191–199.
53 G. Karmakar, A. Tyagi, A. Wadawale, G. Kedarnath, A. P. Srivastava, C. A. Betty and V. Singh, *ChemistrySelect*, 2018, **3**, 10394–10401.
54 Y. Zhao, H. Pan, Y. Lou, X. Qiu, J. Zhu and C. Burda, *J. Am. Chem. Soc.*, 2009, **131**, 4253–4261.
55 A. Kundu and B. Chakraborty, *JACS Au*, 2024, **4**, 642–656.
56 Y. Q. Liu, F. X. Wang, Y. Xiao, H. D. Peng, H. J. Zhong, Z. H. Liu and G. B. Pen, *Sci. Rep.*, 2014, **4**, 5998.
57 M. K. Pal, G. Karmakar, A. Y. Shah, A. Tyagi, N. Bhuvanesh and S. Dey, *New J. Chem.*, 2023, **47**, 16954–16963.